Contribution No. 6321 from the Arthur Amos Noyes Laboratory of Chemical Physics, California Institute of Technology, Pasadena, California 91125, and Contribution from the School of Chemical Sciences, University of Illinois, Urbana, Illinois 61801

Synthesis, Physical Properties, and Crystal Structure of the Cubane Compound Bis(μ-acetato)-tetra-μ-methoxo-bis[μ-(2,5-dimethyl-2,5-diisocyanohexane)]-tetranickel-(II) Tetraphenylborate

WAYNE L. GLADFELTER,[1] MICHAEL W. LYNCH,[2] WILLIAM P. SCHAEFER,[1] DAVID N. HENDRICKSON,*[2] and HARRY B. GRAY*[1]

Received October 10, 1980

Reaction of nickel(II) acetate with 2,5-dimethyl-2,5-diisocyanohexane (TMB) in methanol followed by precipitation with sodium tetraphenylborate produces a compound having the formulation $[Ni_4(OCH_3)_4(OAc)_2(TMB)_4](BPh_4)_2$. A single-crystal X-ray structural analysis reveals that the complex cation adopts a cubane arrangement of nickel(II) and methoxide ions; the acetates bridge two nickel ions on opposite faces of the cube, and the isocyanides bridge the remaining four faces, with each nickel(II) in a distorted octahedral ligand environment. At room temperature $[Ni_4(OCH_3)_4(OAc)_2(TMB)_4](BPh_4)_2$ is paramagnetic, but variable-temperature (286–4.2 K) magnetic susceptibility measurements show that the compound has a diamagnetic ground state. The magnetic exchange among the four $^3A_2$ Ni(II) centers has been modeled with use of three exchange parameters, two ferromagnetic interactions (J_2 = 17.7 and J_3 = 17.2 cm^{-1}) and one antiferromagnetic interaction (J_1 = −9.1 cm^{-1}). It is proposed that these magnetic exchange interactions are propagated by the bridging methoxides and are critically dependent on the Ni–O–Ni angles. The presence of the acetate bridges leads to two types of Ni–O–Ni angles, those that are ca. 93° and those that are ca. 101°. It is suggested that the Ni–O–Ni units possessing the larger angles are coupled antiferromagnetically and that the ferromagnetic interaction is associated with the smaller angles.

Introduction

There are relatively few well-characterized isocyanonickel(II) complexes, owing to the fact that nickel(II) is the most active transition-metal catalyst for the polymerization of isocyanides.[3] As part of our research on polynuclear isocyanide complexes,[4] we have explored the reactions of 1,3-diisocyanopropane (bridge), 2,5-dimethyl-2,5-diisocyanohexane (TMB), and 1,8-diisocyano-*p*-menthane (DMB) with various

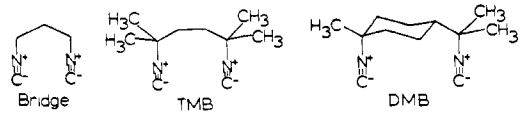

nickel salts. Although bridge was immediately polymerized by all of the salts, TMB and particularly DMB formed stable complexes. The complexes obtained with $NiCl_2$, $NiBr_2$, and $Ni(ClO_4)_2$ will be reported elsewhere. In this paper the unique chemistry that resulted from the addition of TMB or DMB to $Ni(OAc)_2$ in methanol is described. Instead of the expected binuclear product, a tetranuclear species that incorporated solvent into a cubane $Ni_4(OCH_3)_4^{4+}$ framework was formed.

Magnetic susceptibility data in the range of room to liquid-nitrogen temperature have been reported for at least seven different cubane $Ni_4(OCH_3)_4^{4+}$ complexes.[5] Data have also been recorded down to liquid-helium temperature for two of these complexes, $Ni_4(OCH_3)_4(acac)_4(CH_3OH)_4$[6] (acac is acetylacetonate anion) and $Ni_4(OCH_3)_4(sal)_4(C_2H_5OH)$[7] (sal is the monoanion of salicylaldehyde). All of the complexes exhibit ferromagnetic *intra*molecular exchange interactions (J = 3–11 cm^{-1}), a result that has been attributed[5] to the fact that methoxy bridges afford Ni–O–Ni angles in the range of 90 ± 14°. In the case of $Ni_4(OCH_3)_4(acac)_4(CH_3OH)_4$, Ginsberg proposed[5] that *inter*molecular ferromagnetic interactions (as characterized by a Weiss constant of Θ = +0.8°) were present. However, more recent work (heat capacity measurements from 285 to 0.5 K) has shown[8] that cooperative spin ordering does not occur in this compound; thus, *inter*molecular ferromagnetic exchange interaction cannot be very significant. In the present paper, X-ray structural and magnetic susceptibility results are presented for $[Ni_4(OCH_3)_4(TMB)_4(OAc)_2](BPh_4)_2$. The magnetic properties of this compound are significantly different from those exhibited by other $Ni_4(OCH_3)_4^{4+}$ systems; this interesting behavior is probably related to the unusual Ni–O–Ni angles observed in the cubane framework, as discussed herein.

Experimental Section

Ligand Preparations. 2,5-Diisocyano-2,5-dimethylhexane (TMB) and 1,8-diisocyano-*p*-menthane (DMB) were prepared from the corresponding diamines by methods reported previously.[4]

$[Ni_4(OCH_3)_4(TMB)_4(OAc)_2](BPh_4)_2$. TMB (2.082 g, 12.7 mmol) dissolved in 100 mL of MeOH was added slowly to a 150-mL stirred MeOH solution of nickel acetate tetrahydrate (3.16 g, 12.7 mmol). The resultant blue solution was stirred for an additional 10 min, after which a MeOH solution (50 mL) of $NaBPh_4$ (2.169 g, 6.4 mmol) was added slowly. This resulted in the precipitation of a pale blue microcrystalline product. The solution was cooled with ice and filtered, and the solid was air-dried. The initial crop contained 4.195 g of product. Allowing the filtrate to stand overnight resulted in a second crop (0.687 g) that increased the total yield to 4.882 g (2.75 mmol, 87%). Anal. Calcd for $[Ni_4(OMe)_4(TMB)_4(OAc)_2](BPh_4)_2$: C, 65.04; N, 6.32; H, 6.95. Found: C, 64.83; N, 6.11; H, 6.95.

$[Ni_4(OCH_3)_4(DMB)_4(OAc)_2](BPh_4)_2$. This compound was prepared by the same procedure used for its TMB analogue. Anal. Calcd for

(1) California Institute of Technology.
(2) University of Illinois.
(3) Drenth, W.; Nolte, R. J. M. *Acc. Chem. Res.* **1979**, *12*, 30.
(4) (a) Milder, S.; Goldbeck, R.; Kliger, D.; Gray, H. B. *J. Am. Chem. Soc.* **1980**, *102*, 6761. (b) Sigal, I. S.; Mann, K. R.; Gray, H. B. *Ibid.* **1980**, *102*, 7252. (c) Gladfelter, W. L.; Gray, H. B. *Ibid.* **1980**, *102*, 5909. (d) Sigal, I. S.; Gray, H. B. *Ibid.* **1981**, *103*, 2220. (e) Mann, K. R.; Lewis, N. S.; Miskowski, V. M.; Erwin, D. K.; Hammond, G. S.; Gray, H. B. *Ibid.* **1977**, *99*, 5525. (f) Gray, H. B.; Mann, K. R.; Lewis, N. S.; Thich, J. A.; Richman, R. M. *Adv. Chem. Ser.* **1978**, *No.* **168**, 44. (g) Mann, K. R.; Gray, H. B. *Ibid.* **1979**, *No. 173*, 225. (h) Miskowski, V. M.; Sigal, I. S.; Mann, K. R.; Gray, H. B.; Milder, S. J.; Hammond, G. S.; Ryason, P. R. *J. Am. Chem. Soc.* **1979**, *101*, 4383. (i) Gray, H. B.; Miskowski, V. M.; Milder, S. M.; Smith, T. P.; Maverick, A. W.; Buhr, J. D.; Gladfelter, W. L.; Sigal, I. S.; Mann, K. R. *Fundam. Res. Homogeneous Catal.* **1979**, *3*, 819. (j) Miskowski, V. M.; Nobinger, G. L.; Kliger, D. S.; Hammond, G. S.; Lewis, N. S.; Mann, K. R.; Gray, H. B. *J. Am. Chem. Soc.* **1978**, *100*, 485. (k) Mann, K. R; Thich, J. A.; Bell, R. A.; Coyle, C. G.; Gray, H. B. *Inorg. Chem.* **1980**, *19*, 2462. (l) Mann, K. R.; Bell, R. A.; Gray, H. B. *Ibid.* **1979**, *18*, 2671. (m) Mann, K. R.; Lewis, N. S.; Williams, R. M.; Gray, H. B.; Gordon, J. G. *Ibid.* **1978**, *17*, 828. (n) Lewis, N. S.; Mann, K. R.; Gordon, J. G.; Gray, H. B. *J. Am. Chem. Soc.* **1976**, *98*, 7461. (o) Mann. K. R.; Gordon, J. G.; Gray, H. B. *Ibid.* **1975**, *97*, 3553.
(5) Ginsberg, A. P. *Inorg. Chim. Acta, Rev.* **1971**, *5*, 45.
(6) Bertrand, J. A.; Ginsberg, A. P.; Kaplan, R. I.; Kirkwood, C. E.; Martin, R. L.; Sherwood, R. C. *Inorg. Chem.* **1971**, *10*, 240.
(7) Barnes, J. A.; Hatfield, W. E. *Inorg. Chem.* **1971**, *10*, 2355.
(8) Sorai, M.; Yoshikawa, M.; Arai, N.; Suga, H.; Seki, S. *J. Phys. Chem. Solids* **1978**, *39*, 413.

0020-1669/81/1320-2390$01.25/0

Table I. X-ray Data for $[Ni_4(OMe)_4(TMB)_4(OAc)_2](BPh_4)_2 \cdot 4CH_2Cl_2$

(A) Crystal Parameters at 20 °C

cryst system: monoclinic	$V = 11\,206\ (8)$ Å^3
space group: $C2/c$ (No. 15)	$Z = 4$
$a = 28.883\ (20)$ Å	mol wt = 2112.46
$b = 19.664\ (4)$ Å	ρ(measd) = 1.22 g cm^{-3}
$c = 20.99\ (5)$ Å	ρ(calcd) = 1.25 g cm^{-3}
$\beta = 109.95\ (4)°$	$\mu = 8.63$ cm^{-1}

(B) Measurement of Intensity Data

diffractometer: Syntex $P2_1$
radiation: Mo K$\bar{\alpha}$ (λ 0.710 73 Å)
monochromator: graphite
scan type: θ–2θ
2θ range: 0–40°
scan speed: 2°/min in 2θ
scan width: $[2\theta(\text{Mo K}\alpha_1) - 1.0]°$ to $[2\theta(\text{Mo K}\alpha_2) + 1.0]°$
bkgd measurement: fixed θ–2θ for 30 s at each end of each scan
std reflctns: 020, 113, 600 measd every 50 reflections
reflctns measd: 5266 unique; $+h, +k, \pm l$

$[Ni_4(OMe)_4(DMB)_4(OAc)_2](BPh_4)_2$: C, 67.83; N, 5.97; H, 7.00. Found: C, 66.34; N, 6.18; H, 7.08.

Physical Measurements. UV–vis spectra were recorded on a Cary 17 spectrophotometer; IR spectral measurements were made on a Beckman IR-4240 spectrophotometer. Variable-temperature (4.2–286 K) magnetic susceptibility measurements were made with a Princeton Applied Research 150A vibrating-sample magnetometer operated at 13.5 kG. The sample temperature was monitored with a calibrated GaAs temperature-sensitive diode in conjunction with a $CuSO_4 \cdot 5H_2O$ standard. Least-squares computer fittings of the magnetic susceptibility data were performed with a modified version of the function minimization program STEPT.[9]

Crystal Structure Deterimination. Crystals of the TMB complex were grown by adding an equal volume of ethanol to a CH_2Cl_2 solution of the solid. The CH_2Cl_2 was allowed to evaporate slowly in a closed beaker. The beautiful transparent blue crystals that formed could not be removed from a CH_2Cl_2 atmosphere for more than a few minutes before crumbling and apparently losing solvent. Reasonable crystals were plucked from the side of the beaker and quickly coated with fast-drying epoxy. The crystals were subsequently mounted on a glass fiber and recoated with epoxy. The crystal used for intensity data collection was rhombohedral with dimensions 0.44 × 0.49 × 0.61 mm.

Oscillation and Weissenberg photographs gave preliminary cell dimensions and indicated the crystal was monoclinic, having $m/2$ Laue symmetry. The systematic absences for hkl, $h + k = 2n + 1$, $h0l$, $l = 2n + 1$, and $0k0$, $k = 2n + 1$, indicated two possible space groups: the noncentrosymmetric Cc (C_s^4; No. 9) or the centrosymmetric $C2/c$ (C_{2h}^6; No. 15). Accurate cell dimensions were obtained from the setting angles of 15 reflections accurately centered on a Syntex $P2_1$ diffractometer. These results and the details of the data collection procedure are given in Table I.

The data were corrected for Lorentz and polarization effects but not for absorption ($\mu = 8.63$ cm^{-1}). During data collection, the three check reflections showed an average intensity decrease of 1.7%. The intensities of all the reflections were corrected for this decay. Standard deviations were assigned to each measurement on the basis of counting statistics plus an additional factor, $(0.02I)^2$, to account for fluctuations proportional to the diffracted intensity.

Solution and Refinement of the Structure. Statistical tests of the data by the method of Howells, Phillips, and Rogers indicated the structure was centrosymmetric.[10] Accordingly, refinement proceeded with the use of the space group $C2/c$. All calculations were done on an IBM 370/168 machine using programs of the CRYM crystallographic computing system. Scattering factors for Ni, Cl, O, N, C, and B were taken from ref 11, the values for Ni being increased by 0.37 electron and for Cl by 0.15 electron to account for the effects of anomalous dispersion. The hydrogen scattering factors are those of Stewart, Davidson, and Simpson[12] for bonded hydrogen. The structure was solved by Patterson and Fourier techniques. Some difficulty in interpreting the Patterson maps arose from the similar peak heights of the Ni–Ni vectors and the large number of superimposed Ni–ligand (C and O) vectors, but the Ni atoms and some of the carbon and oxygen atoms in the coordination sphere were located. The remaining atoms in the asymmetric unit were located by successive structure factor–Fourier calculations. It was apparent at this stage that there were two solvent areas in the asymmetric unit that were badly disordered. Although we believed that these areas contained CH_2Cl_2, the electron density seemed too small; therefore, only C atoms were placed in these positions, and refinement continued. Four cycles of blocked isotropic matrix least-squares refinement using 3300 low-angle ($(\sin^2\theta)/\lambda^2 < 0.17$) reflections resulted in an R value of 0.171. One matrix contained all of the atomic coordinates, and the other contained the temperature factors and scale factor. At this stage, one of the solvent regions appeared to contain a recognizable CH_2Cl_2, which was refined anisotropically along with the Ni atoms. This lowered the R value to 0.127. A difference Fourier using the low-angle data ($(\sin^2\theta)/\lambda^2 < 0.12$) showed several of the hydrogen atoms bound to the methyl carbon atoms. The positions of the hydrogen atoms of the methylene and phenyl groups were calculated by using C(phenyl)–H = 1.08 Å and C(methylene)–H = 1.073 Å. The temperature factors were assigned as $B(H) = B(C) + 1.0$. Inclusion of the hydrogen atoms (not refined) and anisotropic refinement of the oxygen atoms, solvent (both regions), and methyl carbon atoms resulted in an R value of 0.107 after several least-squares cycles.

At this stage a difference Fourier map indicated that the only problem was in the solvent regions. We attempted to model the disordered solvent regions using CH_2Cl_2 molecules with the only constraint being that the model should be chemically reasonable. All atoms were removed from these areas, and a structure factor calculation was performed ($R = 0.192$). From the Fourier maps of these regions were obtained positions for three orientations of a CH_2Cl_2 molecule in region 1 and four orientations of a CH_2Cl_2 molecule in region 2. Each area was initially given a total population of 0.5. The populations, positions and isotropic thermal parameters were refined by using difference Fourier techniques only. After seven cycles of structure factor–difference Fourier calculations region 1 was fitted with five orientations of a CH_2Cl_2 molecule with a total population of 0.94, and region 2 was fitted with four orientations of a CH_2Cl_2 molecule with a total population of 0.72. The largest positive peak in the final difference Fourier map of region 1 was 0.59 e/Å^3, while the largest negative peak was –0.91 e/Å^3. In region 2, the range was +0.82 to –0.65 e/Å^3. The R value at this point was 0.090. The solvent atom positions, populations, and temperature factors were not allowed to refine in any subsequent least-squares refinement.

Two cycles of least-squares calculations treating most of the remaining atoms anisotropically lowered the R value to 0.087. All of the hydrogen atom positions were recalculated or relocated in the areas of the methyl groups. Examination of the calculated and observed structure factors indicated several large residuals for the low-angle data. These low-angle data are more sensitive to the disordered solvent regions than the high-angle data, due to the more rapid decrease in the scattering factors of these atoms. In an effort to minimize the effect of the solvent regions on the remainder of the structure during the last cycles of least-squares refinement, all data with $(\sin^2\theta)/\lambda^2 < 0.02$ (134 reflections) were removed. At the same time the remaining 2000 high-angle reflections were added to the data set, bringing the total number to 5132. After two cycles of least-squares refinement all parameters converged, giving a final R value of 0.099 and $R_w = 0.13$. [$R = (\sum||F_o| - |F_c||/\sum F_o)$; $R_w = (\sum w(F_o^2 - F_c^2)^2/\sum wF_o^4)^{1/2}$; GOF = $(\sum w(F_o^2 - F_c^2)^2/(N_o - N_p))^{1/2}$, where N_o is the number of data and N_p the number of parameters.] The goodness of fit was 1.83. The last cycle included a summation of the intensity data with $F_o^2 > 3\sigma(F_o^2)$ and yielded an R (>3σ) value of 0.062. The refined positional and thermal heavy-atom parameters are set out in Table II. The solvent and hydrogen parameters and a listing of observed and calculated structure factors are given in the supplementary material.

Magnetic Susceptibility Theory

The magnetic susceptibility characteristics of tetranuclear clusters have been reviewed previously.[5,13] In general, the

(9) Chandler, J. P. Quantum Chemistry Program Exchange, Indiana University, Bloomington, Ind; Program 66.
(10) Howell, E. R.; Phillips, D. C.; Rogers, D. *Acta Crsytallogr.* **1950**, *3*, 210.
(11) "International Tables for X-ray Crystallography"; Kynoch Press: Birmingham, England, 1962; Vol. III, p 202.
(12) Stewart, R. F.; Davidson, E. R.; Simpson, W. T. *J. Chem. Phys.* **1965**, 42, 3175.

Table II. Refined Heavy-Atom Parameters[a]

atom	x	y	z	U_{11} [or B, Å^2]	U_{22}	U_{33}	U_{12}	U_{13}	U_{23}
NiA	4759 (0.4)	4821 (0.5)	3080 (0.5)	42 (0.7)	36 (0.7)	42 (0.7)	5 (0.6)	6 (0.5)	−5 (0.6)
NiB	4494 (0.4)	3745 (0.5)	1871 (0.5)	49 (0.7)	36 (0.7)	41 (0.7)	−8 (0.6)	14 (0.5)	−5 (0.6)
NA1	3648 (3)	4975 (3)	3048 (3)	53 (5)	63 (5)	43 (4)	1 (4)	14 (4)	−2 (4)
NA2	4861 (2)	6435 (4)	3293 (4)	64 (5)	51 (6)	82 (6)	6 (5)	6 (4)	−10 (5)
NB1	3373 (3)	3608 (3)	1799 (3)	55 (5)	53 (5)	57 (5)	−13 (4)	13 (4)	−2 (4)
NB2	4543 (3)	2135 (4)	1661 (4)	75 (6)	50 (6)	116 (7)	−15 (5)	44 (5)	−21 (5)
O1	4558 (2)	4778 (2)	2033 (2)	42 (3)	33 (3)	35 (3)	1 (3)	3 (3)	1 (3)
O2	4752 (2)	3782 (2)	2922 (2)	47 (3)	36 (3)	38 (3)	−1 (3)	15 (3)	−1 (3)
O3	5075 (2)	4685 (3)	4097 (2)	56 (4)	65 (4)	32 (4)	20 (3)	3 (3)	−7 (3)
O4	4357 (2)	3884 (3)	854 (2)	62 (4)	66 (4)	40 (4)	−25 (3)	15 (3)	−4 (3)
CA1	4045 (3)	4857 (4)	3098 (4)	48 (6)	59 (6)	46 (6)	5 (5)	10 (5)	−6 (5)
CA2	3115 (3)	5146 (5)	2877 (4)	38 (6)	101 (8)	61 (6)	3 (6)	19 (5)	−7 (6)
CA3	2988 (3)	5039 (6)	3521 (5)	58 (6)	137 (10)	91 (8)	6 (7)	36 (6)	−16 (7)
CA4	3059 (3)	5887 (5)	2660 (5)	64 (7)	71 (7)	105 (8)	30 (6)	9 (6)	3 (6)
CA5	2831 (3)	4680 (5)	2293 (4)	43 (6)	81 (7)	65 (7)	6 (5)	16 (5)	−1 (6)
CA6	4804 (3)	5865 (5)	3189 (4)	48 (6)	52 (6)	63 (7)	3 (5)	−3 (5)	−7 (6)
CA7	4984 (4)	7180 (5)	3416 (6)	118 (10)	37 (7)	140 (12)	−21 (7)	20 (9)	−23 (7)
CA8	388 (5)	2200 (7)	4119 (6)	118 (13)	121 (11)	106 (10)	−64 (10)	0 (9)	−48 (9)
CA9	491 (5)	2539 (6)	1616 (7)	173 (13)	62 (8)	204 (14)	−14 (8)	77 (11)	43 (9)
CA10	187 (4)	2378 (5)	2857 (5)	109 (11)	53 (7)	138 (11)	−26 (6)	28 (7)	−8 (6)
CB1	3754 (3)	3708 (4)	1770 (4)	54 (6)	56 (6)	54 (6)	−6 (5)	17 (5)	−4 (5)
CB2	2899 (3)	3458 (5)	1912 (5)	49 (7)	77 (7)	90 (8)	−21 (6)	22 (6)	9 (6)
CB3	2476 (3)	3557 (6)	1238 (5)	57 (7)	135 (10)	90 (8)	−13 (7)	13 (6)	−16 (7)
CB4	2939 (4)	2702 (5)	2139 (6)	118 (9)	81 (8)	133 (10)	−38 (7)	70 (8)	−18 (7)
CB5	2878 (3)	3918 (5)	2486 (4)	61 (6)	97 (8)	59 (7)	−18 (6)	25 (5)	−1 (6)
CB6	4504 (3)	2698 (4)	1761 (4)	63 (6)	42 (6)	75 (7)	−16 (5)	34 (5)	−5 (5)
CB7	4649 (4)	1414 (5)	1539 (7)	117 (11)	45 (8)	167 (12)	−7 (7)	60 (9)	−49 (8)
CB8	4165 (4)	1024 (5)	1427 (8)	109 (10)	47 (7)	271 (18)	−19 (7)	6 (10)	−43 (9)
CB9	4815 (5)	1403 (7)	913 (8)	161 (13)	154 (13)	191 (15)	18 (10)	47 (11)	−109 (12)
CB10	5062 (4)	1183 (4)	2180 (6)	82 (8)	42 (6)	187 (14)	2 (7)	33 (9)	−38 (7)
C1	4164 (3)	5210 (4)	1629 (4)	53 (6)	58 (6)	55 (6)	−5 (5)	10 (5)	6 (5)
C2	4527 (3)	3353 (4)	3296 (4)	67 (6)	47 (6)	54 (6)	6 (5)	29 (5)	5 (5)
C3	4576 (3)	4294 (5)	601 (4)	58 (7)	92 (8)	33 (6)	−15 (6)	1 (5)	6 (5)
C4	4402 (4)	4315 (7)	−180 (5)	131 (10)	186 (13)	37 (6)	−87 (9)	8 (6)	−9 (7)
B	3515 (4)	967 (5)	4613 (5)	[4.5 (2)]					
C20	91 (4)	4390 (5)	4242 (5)	[6.1 (2)]					
C21	530 (4)	4327 (5)	4815 (5)	[5.6 (2)]					
C22	976 (3)	4182 (4)	4736 (4)	[4.3 (2)]					
C23	975 (3)	4103 (4)	4081 (5)	[5.1 (2)]					
C24	545 (4)	4164 (5)	3509 (5)	[5.8 (2)]					
C25	111 (4)	4321 (4)	3613 (5)	75 (7)	46 (6)	95 (8)	−8 (5)	−3 (6)	12 (5)
C26	3533 (4)	13 (9)	2700 (6)	75 (9)	207 (16)	87 (10)	−15 (10)	20 (7)	−73 (10)
C27	3397 (4)	971 (6)	3280 (5)	88 (8)	162 (11)	57 (7)	0 (8)	28 (6)	−12 (7)
C28	3544 (3)	625 (5)	3896 (5)	[6.0 (2)]					
C29	3398 (4)	678 (8)	2684 (6)	102 (10)	198 (16)	79 (9)	−22 (10)	29 (8)	3 (10)
C30	3677 (3)	−43 (6)	3899 (5)	53 (6)	120 (10)	99 (9)	−9 (6)	15 (6)	−46 (7)
C31	3682 (4)	−365 (7)	3282 (7)	60 (8)	169 (13)	139 (12)	3 (8)	12 (8)	−65 (11)
C32	3033 (3)	598 (4)	4718 (4)	[4.6 (2)]					
C33	2552 (4)	819 (5)	4317 (4)	[5.6 (2)]					
C34	2136 (4)	512 (5)	4371 (5)	[6.6 (3)]					
C35	2174 (3)	−19 (5)	4807 (5)	63 (7)	96 (8)	100 (8)	−25 (6)	36 (6)	−38 (7)
C36	2631 (4)	−264 (6)	5200 (5)	96 (9)	99 (9)	94 (9)	−16 (7)	43 (7)	3 (7)
C37	3054 (3)	48 (5)	5146 (4)	[5.5 (2)]					
C38	3465 (3)	1784 (5)	4564 (4)	[5.1 (2)]					
C39	3766 (4)	2198 (6)	4314 (5)	85 (8)	100 (8)	90 (8)	−9 (7)	45 (7)	12 (7)
C40	3746 (4)	2910 (7)	4315 (6)	123 (11)	101 (10)	120 (11)	−26 (8)	57 (8)	37 (9)
C41	3444 (5)	3240 (6)	4605 (6)	113 (11)	94 (10)	119 (11)	11 (8)	31 (8)	47 (8)
C42	3161 (4)	2862 (6)	4851 (6)	82 (9)	95 (9)	129 (11)	11 (7)	38 (8)	10 (8)
C43	3169 (4)	2155 (5)	4833 (5)	84 (8)	68 (7)	109 (9)	7 (6)	39 (7)	3 (7)

[a] Coordinates have been multiplied by 10^4; U_{ij} values, by 10^3.

magnetic exchange interactions between nearest-neighbor metal ions in the cluster are treated with an isotropic spin Hamiltonian

$$\hat{H} = -2\sum J_{ij}\hat{S}_i\cdot\hat{S}_j \qquad (1)$$

where J_{ij} is the exchange parameter between the ith and jth paramagnetic ions and $\hat{S}_i$ and $\hat{S}_j$ are spin operators on the ions. The vector-coupling model[14] is used to derive the eigenvalues for a particular complex. The *intra*molecular magnetic exchange interactions present in $[Ni_4(OCH_3)_4(TMB)_4(OAc)_2](BPh_4)_2$ are largely due to interactions between $^3A_2$ nickel(II) ions as propagated by bridging methoxides. Direct exchange interactions between nickel(II) ions should be negligible. It is the geometry in the $Ni_4(OCH_3)_4^{4+}$ cubane structure (vide infra) that determines the nature of the magnetic exchange interactions that are seen. Two of the three theoretical models used to fit the susceptibility data can be understood by reference to the diagram

(13) Martin, R. L. "New Pathways in Inorganic Chemistry"; Cambridge University Press: London, 1968; Chapter 9, p 175.

(14) Kambe, K. *J. Phys. Soc. Jpn.* **1950**, *5*, 48.

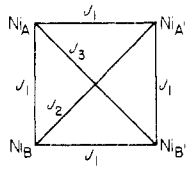

Ginsberg et al. derived[6] the magnetic susceptibility expression for such a nickel(II) cubane structure, assuming that all pairwise interactions are equal (i.e., $J_1 = J_2 = J_3$). The susceptibility/mol of cubane cluster, χ_M, is given in eq 2, where

$$\chi_M = \frac{4g^2N\beta^2}{kT}\left[\frac{5e^{20x} + 7e^{12x} + 5e^{6x} + e^{2x}}{3e^{20x} + 7e^{12x} + 10e^{6x} + 6e^{2x} + 1}\right] + N\alpha \quad (2)$$

$x = J/kT$ and $N\alpha$ is the term added to take account of the temperature-independent paramagnetism. In all models $N\alpha$ was taken to be 400×10^{-6} cgsu/tetranuclear cluster. The other symbols have their usual meanings.

If it is assumed that the three exchange parameters in the preceding diagram are not equal (i.e., $J_1 \neq J_2 \neq J_3$), then the spin Hamiltonian operator describing the magnetic exchange in the cubane cluster can be written as shown in eq 3. The vector-coupling method of Kambe[14] was used to obtain

$$\hat{H} = -2J_1(\hat{S}_A\cdot\hat{S}_{A'} + \hat{S}_A\cdot\hat{S}_B + \hat{S}_B\cdot\hat{S}_{B'} + \hat{S}_{A'}\cdot\hat{S}_{B'}) - 2J_2(\hat{S}_{A'}\cdot\hat{S}_B) - 2J_3(\hat{S}_A\cdot\hat{S}_{B'}) \quad (3)$$

the eigenvalues for this spin Hamiltonian; the eigenvalues are

$$E(S_T,S_K,S_L) = -J_1[S_T(S_T + 1)] - (J_2 - J_1) \times [S_K(S_K + 1)] - (J_3 - J_1)[S_L(S_L + 1)] + 4(J_2 + J_3) \quad (4)$$

In this expression, the total spin is given as $S_T = S_K + S_L$, $S_K = S_{A'} + S_B$, and $S_L = S_A + S_{B'}$. A general form of the above equation for a cubane array of metal ions with any spin was derived by Dubicki et al.[15] There are 19 different energy levels for the $J_1 \neq J_2 \neq J_3$ case, and the eigenvalues of the 19 levels can be calculated from eq 4. The magnetic susceptibility/mol of cubane cluster is given as shown in eq 5. The values for the coefficients a_i and b_i are given in Table III.

$$\chi_M = \frac{g^2N^2}{3kT}\left[\frac{\sum_{i=1}^{19} a_i \exp(-E_i/kT)}{\sum_{i=1}^{19} b_i \exp(-E_i/kT)}\right] + N\alpha \quad (5)$$

In addition to the above two cubane models, the data for $[Ni_4(OCH_3)_4(TMB)_4(OAc)_2](BPh_4)_2$ were also least-squares fit to a susceptibility expression for two noninteracting nickel(II) dimers:[16]

$$\chi_M = \frac{2g^2N\beta^2}{3kT}\left[\frac{30\exp(6J/kT) + 6\exp(2J/kT)}{5\exp(6J/kT) + 3\exp(2J/kT) + 1}\right] + N\alpha \quad (6)$$

Results and Discussion

The structure of $[Ni_4(OCH_3)_4(TMB)_4(OAc)_2]^{2+}$ is shown in Figure 1. Each unit cell contains four such cubane clusters (Figure 2) situated in the special position along the C_2 axis. The C_2 axis intersects the center of the NiB–O2–NiB′–O2′ and the NiA–O1–NiA′–O1′ faces. The overall symmetry of the cluster is greater than C_2 and with small deviations fits the point group D_{2d}. The numbering sequence for the isocyanide ligands is shown in Figure 3. Bond distances and angles are summarized in Tables IV and V, respectively.

(15) Dubicki, L.; Kakos, G. A.; Winter, G. *Aust. J. Chem.* **1968**, *21*, 1461.
(16) Duggan, D. M.; Barefield, E. K.; Hendrickson, D. N. *Inorg. Chem.* **1973**, *12*, 985.

Table III. Coefficients for the Susceptibility Equation (5)

E_i	S_K	S_L	M_{ST}	a_i	b_i
1	2	2	4	180	9
2	2	2	3	84	7
3	2	2	2	30	5
4	2	2	1	6	3
5	2	2	0	0	1
6	2	1	3	84	7
7	2	1	2	30	5
8	2	1	1	6	3
9	1	2	3	84	7
10	1	2	2	30	5
11	1	2	1	6	3
12	2	0	2	30	5
13	0	2	2	30	5
14	1	1	2	30	5
15	1	1	1	6	3
16	1	1	0	0	1
17	1	0	1	6	3
18	0	1	1	6	3
19	0	0	0	0	1

Table IV. Bond Distances (Å)

NiA–NiA′	3.190 (1)	NA1–CA2	1.49 (1)
NiB–NiB′	3.202 (1)	NA2–CA7	1.51 (1)
NiA–NiB	3.189 (1)	NB1–CB2	1.50 (1)
NiA–NiB′	2.998 (1)	NB2–CB7	1.49 (1)
NiA–O1	2.074 (5)	N–C (av)	1.50 (1)
NiA–O3	2.032 (5)	CA2–CA5	1.53 (1)
NiA–O2	2.068 (5)	CB2–CB5	1.53 (1)
NiA–O1′	2.068 (5)	CA7–CA10	1.53 (2)
NiB–O1	2.058 (5)	CB7–CB10	1.53 (2)
NiB–O2	2.074 (5)	C–C (av)	1.53 (2)
NiB–O4	2.052 (5)	CA5–CB5	1.55 (1)
NiB–O2′	2.072 (5)	CA10–CA10′	1.52 (1)
NiA–CA1	2.079 (8)	CB10–CB10′	1.50 (2)
NiA–CA6	2.065 (9)	C–C (av)	1.52 (3)
NiB–CB1	2.074 (9)	CA2–CA3	1.53 (1)
NiB–CB6	2.074 (9)	CA2–CA4	1.52 (1)
O1–C1	1.441 (9)	CB2–CB3	1.53 (1)
O2–C2	1.448 (9)	CB2–CB4	1.55 (1)
O–C (av)	1.445 (9)	CB7–CB8	1.54 (2)
O3–C3	1.25 (1)	CB7–CB9	1.55 (2)
O4–C3	1.25 (1)	CA7–CA8	1.54 (2)
O–C (av)	1.25 (1)	CA7–CA9	1.52 (2)
C3–C4	1.54 (1)	C–C (av)	1.54 (2)
CA1–NA1	1.14 (1)	C–C (BPh_4^-) (av)	1.39 (3)
CA6–NA2	1.14 (1)	B–C (BPh_4^-) (av)	1.65 (3)
CB1–NB1	1.14 (1)		
CB6–NB2	1.14 (1)		
C–N (av)	1.14 (1)		

Each acetate ion must extend 2.998 (1) Å between two nickel atoms of the cube, which produces an O3–C3–O4′ angle of 128.1 (8)° and C3–O–Ni angles of 125.5 (5) and 127.4 (5)°. Although these latter angles suggest some asymmetry, each of the two C–O(OAc) distances is 1.25 (1) Å.

There are two independent isocyanide bridges in the cluster. Several features of these bridges are of particular interest. The Ni–C–N angles depart significantly from linearity. The smallest angles of 168.4 (7) and 168.5 (7)° occur on two of the ligands, whereas the other two have angles of 172.4 (8) and 174.6 (8)°. Slightly less bending occurs in the C–N–C angles and they do not vary as greatly as the Ni–C–N angles. The values are 171.8 (8), 174.0 (9), 174.1 (8), and 174.3 (9)°. The C≡N bond length is 1.14 (1) Å in every case. The carbon backbone of each bridging isocyanide exhibits normal bond distances and angles.

Each nickel atom is found in a distorted octahedral environment that includes two cis isocyanide ligands, three

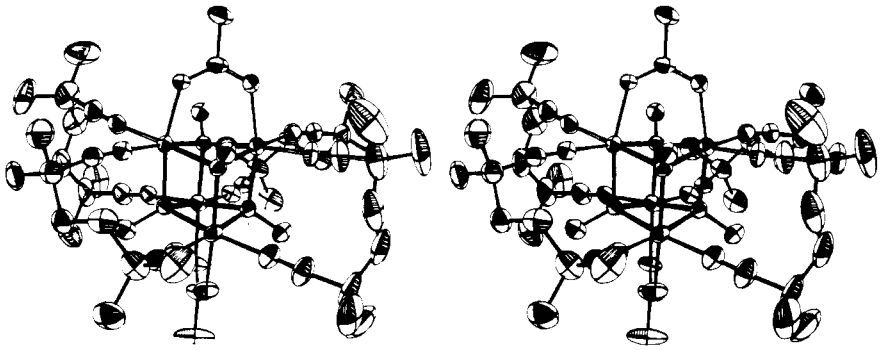

Figure 1. Stereoview of $[Ni_4(OCH_3)(OAc)_2(TMB)_4]^{2+}$. The orientation is similar to that shown in Figure 4.

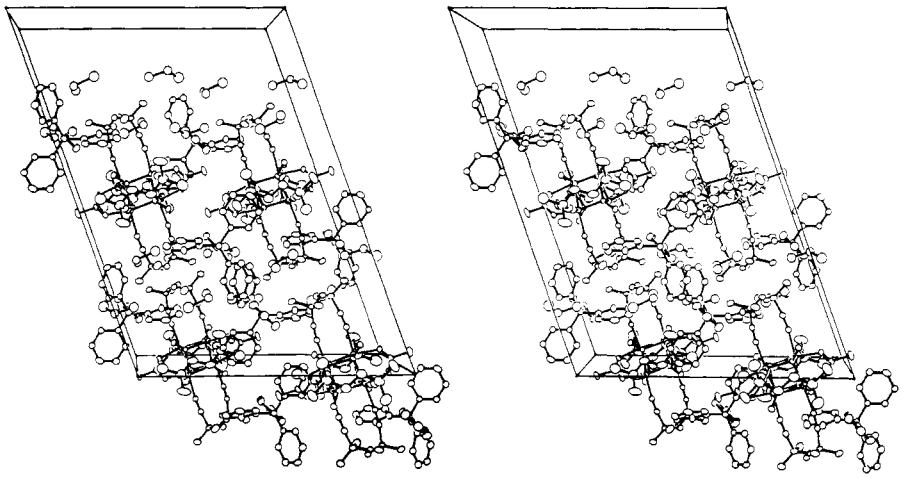

Figure 2. Stereoview of the unit cell contents of $[Ni_4(OCH_3)_4(OAc)_2(TMB)_4](BPh_4)_2 \cdot 4CH_2Cl_2$ as viewed down the y axis with the z axis horizontal.

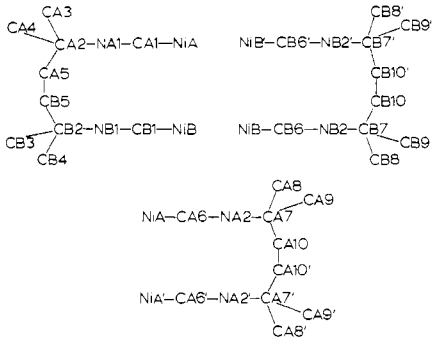

Figure 3. Bridging-isocyanide numbering sequence.

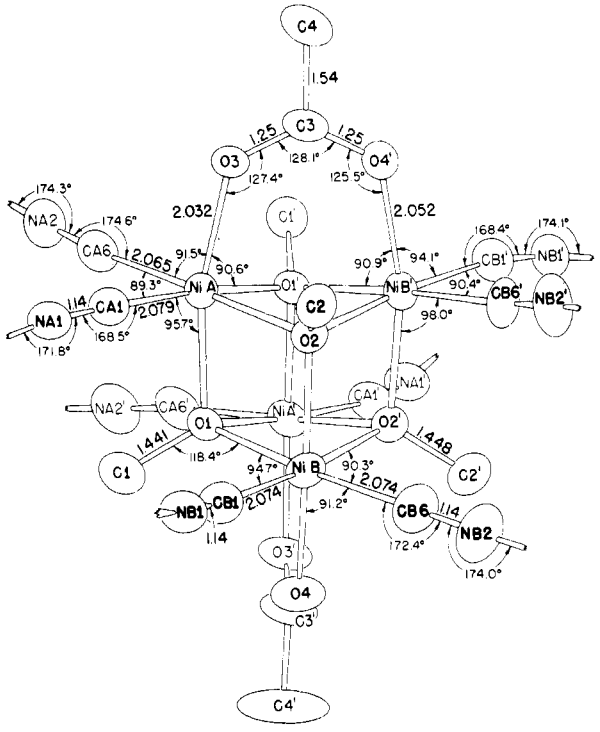

Figure 4. View showing the atom labels and selected distances and angles outside the cube.

methoxide oxygen atoms, and one acetate oxygen atom (Figures 4 and 5). The Ni–donor atom distances differ relatively little among these ligands. The Ni–O(OAc) bonds at 2.032 (5) and 2.052 (5) Å are the shortest. The Ni–O(OCH_3) [2.058 (5)–2.074 (5) Å] and Ni–C bond lengths [2.065 (9)–2.079 (8) Å] are strikingly similar.

If the unique axis about the nickel atom is designated to contain the Ni–O(OAc) bond, then it is this axis about which most of the distortion occurs. The ultimate measure of the distortion is given in the O1–NiA–O3 angle of 166.0 (2)° and the O2–NiB–O4 angle of 166.7 (2)°. As seen in Figure 4, the square plane (referred to as plane A) comprised of NiA–CA6–CA1–O1′–O2 does not bisect the O1–NiA–O3 angle. Plane A is perpendicular to the NiA–O3 bond, whereas the O(OCH_3)–Ni–O(OCH_3) angles such as O2–NiA–O1 are 79°. Also, the C–Ni–O(OCH_3) angles such as CA1–NiA–O1 are 96–98°.

There is less distortion in plane A itself. The ligand–Ni–ligand angles vary from 84.2 (2) to 94.7 (3)°. The smallest angles are O(OCH_3)–Ni–O(OCH_3) and the largest are O(OCH_3)–Ni–C. The C–Ni–C angles are 89.3 (3) and 90.4 (3)°.

The dimensions of the cubane portion of the structure are shown in Figure 5. The distortion of the cube can be viewed as the sum of two distorting modes. First, the four methoxide

Table V. Bond Angles (Deg)

CA1-NiA-CA6	89.3 (3)	O3-C3-O4′	128.1 (8)
CA1-NiA-OA1	95.7 (3)	O3-C3-C4	115.9 (8)
CA1-NiA-O3	94.5 (3)	O4′-C3-C4	116.0 (8)
CA1-NiA-O2	94.7 (3)	NiA-CA1-NA1	168.5 (7)
CA1-NiA-O1′	174.8 (3)	NiA-CA6-NA2	174.6 (8)
CA6-NiA-O1	98.1 (3)	NiB-CB1-NB1	168.4 (7)
CA6-NiA-O3	91.5 (3)	NiB-CB6-NB2	172.4 (8)
CA6-NiA-O2	175.2 (3)	CA1-NA1-CA2	171.8 (8)
CA6-NiA-O1′	91.5 (3)	CA6-NA2-CA7	174.3 (9)
O1-NiA-O3	166.0 (2)	CB2-NB1-CB1	174.1 (8)
O1-NiA-O2	78.8 (2)	CB7-NB2-CB6	174.0 (9)
O1-NiA-O1′	79.1 (2)	CA3-CA2-CA5	113.6 (7)
O3-NiA-O2	90.9 (2)	CA3-CA2-NA1	107.1 (7)
O3-NiA-O1′	90.6 (2)	CA3-CA2-CA4	111.4 (8)
O2-NiA-O1′	84.2 (2)	CA5-CA2-NA1	106.5 (7)
CB1-NiB-CB6	90.4 (3)	CA5-CA2-CA4	111.2 (7)
CB1-NiB-O1	94.7 (3)	C-CA2-C(N) (av)	109 (3)
CB1-NiB-O2	95.4 (3)	NA1-CA2-CA4	106.5 (7)
CB1-NiB-O4	94.1 (3)	NA2-CA7-CA9	106.7 (9)
CB1-NiB-O2′	174.1 (3)	NA2-CA7-CA8	104.2 (9)
CB6-NiB-O1	174.3 (3)	NA2-CA7-CA10	104.2 (8)
CB6-NiB-O2	98.0 (3)	CA9-CA7-CA8	114 (1)
CB6-NiB-O4	91.2 (3)	CA9-CA7-CA10	115 (1)
CB6-NiB-O2′	90.3 (3)	CA8-CA7-CA10	111 (1)
O1-NiB-O2	79.1 (2)	C(N)-CA2-C (av)	109 (5)
O1-NiB-O4	90.9 (2)	CB3-CB2-CB4	110.9 (8)
O1-NiB-O2′	84.4 (2)	CB3-CB2-CB5	114.8 (8)
O2-NiB-O4	166.7 (2)	CB3-CB2-NB1	108.2 (7)
O2-NiB-O2′	78.7 (2)	CB4-CB2-CB5	110.2 (8)
O4-NiB-O2′	91.7 (2)	CB4-CB2-NB1	105.2 (7)
NiA-O1-NiA′	100.7 (2)	CB5-CB2-NB1	107.1 (7)
NiA-O1-NiB	101.0 (2)	C-CB2-C(N) (av)	109 (3)
NiA-O1-C1	118.7 (4)	CB8-CB7-CB9	113 (1)
NiA′-O1-NiB	93.2 (2)	CB8-CB7-NB2	106 (1)
NiA′-O1-C1	120.1 (4)	CB8-CB7-CB10	112 (1)
NiB-O1-C1	118.4 (4)	CB9-CB7-NB2	107 (1)
NiA-O2-NiB	100.7 (2)	CB9-CB7-CB10	112 (1)
NiA-O2-NiB′	92.8 (2)	NB2-CB7-CB10	106.1 (9)
NiA-O2-C2	118.0 (4)	C(N)-CB7-C(N) (av)	109 (3)
NiB-O2-NiB′	101.1 (2)	CA2-CA5-CB5	113.3 (7)
NiB-O2-C2	119.4 (4)	CA5-CB5-CB2	113.1 (7)
NiB′-O2-C2	120.0 (4)	CB7-CB10-CB10′	116 (1)
NiA-O3-C3	127.4 (5)	CA7-CA10-CA10′	115.3 (9)
NiB-O4-C3′	125.5 (5)	C-C-C (BPh_4^-) (av)	120 (3)
		C-C-B (BPh_4^-) (av)	122 (2)
		C-B-C (BPh_4^-) (av)	110 (4)

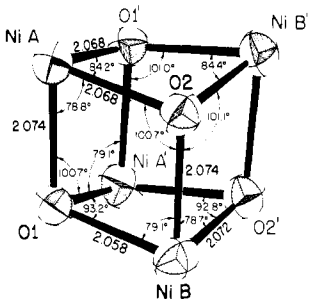

Figure 5. View showing the distances and angles within the central cube.

ions are pushed equally toward the center of the cube, thereby making all of the Ni–O–Ni angles greater than 90° and decreasing the O–Ni–O angles to 78–84°. Second, one of the bridging acetates forces NiA and NiB′ together, whereas the other pinches NiA′ and NiB. This second distortion is smaller in magnitude than the first; it is reflected in the NiA–NiB′ distance of 2.998 (1) Å, which may be compared to the larger average distance of 3.194 (7) Å between nickel ions that are not bridged by acetates. The acetate pinching also produces the observed differences in the three angles about each atom in the cube. For instance, the angles about O2 are 100.7 (2), 101.1 (2), and 92.8 (2)°. The smallest angle (NiA–O2–NiB′) lies in the top half of the cube (i.e., between two nickels bridged by the acetate). Conversely, the angles about NiA are 78.8 (2), 79.1 (2), and 84.2 (2)°. The largest angle of these three is for the O1′–NiA–O2 angle in the top half of the cube. The three Ni–O–C angles about the methoxide oxygen atom are 119 (1)°.

One of the most interesting features of the structure of the tetranuclear cation is the relatively long Ni–C bond distance (~2.07 Å). For comparison, the Ni–C bond length in the only other structurally characterized nickel(II) isocyanide complex, $NiO_2(CN\text{-}t\text{-}Bu)_2$,[17] is ~0.2 Å shorter:

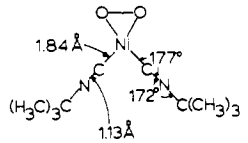

The longer Ni–C bond length in $[Ni_4(OCH_3)_4(TMB)_4(OAc)_2]^{2+}$ is readily explained in terms of the electronic structure of the Ni(II) centers. The presence of a $\sigma^*(d_{x^2-y^2})$ electron in each $^3A_2$ Ni(II) weakens (lengthens) the Ni–C bonds relative to the four-coordinate low-spin Ni(II) complex. The argument is much the same as that used to rationalize the differences in the axial and equatorial Co–C distances in $Co(CN)_5^{3-}$.[18] The extra electron in this d^7 complex occupies an axial $\sigma^*(d_{z^2})$ orbital, which accounts for the observed lengthening (0.12 Å) of the axial Co–C bond.

An important consequence of the Ni–C bond lengthening in the tetranuclear cation is a reduction in π-orbital overlap between the π^* CNR and the Ni $d\pi$ orbitals. The reduced π interaction renders the Ni—C≡N unit more susceptible to bending due to ring strain and intermolecular interactions, thereby resulting in large deviations of the Ni–C–N angle from 180°. The reduced back-bonding is also reflected in the 1.14 Å C≡N bond distance, which is slightly shorter than the usual value of 1.16 Å.

The structures of other compounds that contain a $Ni_4(OMe)_4^{4+}$ cubane core[6,19,20] are in general very similar to that of the TMB complex. The Ni–O bond distances are all in the 2.02–2.12 Å range. The TMB complex, however, is the only one that has bridging ligands other than the μ_3-methoxide. Bertrand and Hightower have prepared $Co_4(OMe)_4(OAc)_2(acac)_4$, which has a similar structure with respect to the metal ions and methoxide and acetate bridges.[21] This cobalt compound is of particular interest because there are two Co(II) and two Co(III) centers. The distances and angles about Co(II) are similar to those of the $Ni_4(OMe)_4^{4+}$ structure. The geometry about Co(III) conforms much more closely to octahedral, however, and the Co–O distances are shortened by 0.15 Å.

The counterion (BPh_4^-) exhibits its normal geometry. Each asymmetric unit also contains two solvent regions. The solvent molecules are badly disordered in both of these areas. This disorder made identification of the solvent molecule difficult (the compound was crystallized from a CH_2Cl_2/EtOH mixture). Two experiments support the presence of CH_2Cl_2 in these sites. First, an infrared spectrum obtained for crystals crushed in Nujol showed the presence of a peak attributable to CH_2Cl_2 at 742 cm^{-1}. In the second experiment, freshly prepared crystals were placed in a mass spectrometer. After

(17) Matsumoto, M.; Nakatsu, K. *Acta Crystallogr., Sect. B* **1975**, *B31*, 2711.
(18) Brown, L. D.; Raymond, K. N. *Inorg. Chem.* **1975**, *14*, 2590.
(19) Andrew, J. E.; Blake, A. B. *J. Chem. Soc. A* **1969**, 1456.
(20) Bertrand, J. A.; Marabella, C.; Vanderveer, D. G. *Inorg. Chim. Acta* **1978**, *26*, 113.
(21) Bertrand, J. A.; Hightower, T. C. *Inorg. Chem.* **1973**, *12*, 206.

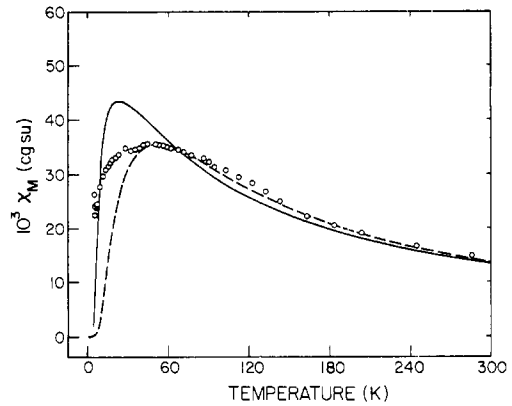

Figure 6. Plot of molar paramagnetic susceptibility vs. temperature for $[Ni_4(OCH_3)_4(TMB)_4(OAc)_2](BPh_4)_2$. Least-squares fits to two different theoretical models are illustrated. The solid line results from fitting to eq 6 (two noninteracting dimers) to give $J = -18$ cm^{-1} and $g = 2.16$. The dashed line represents a fit to eq 2 (cubane cluster with one exchange parameter) to give $J = 10$ cm^{-1} and $g = 2.20$.

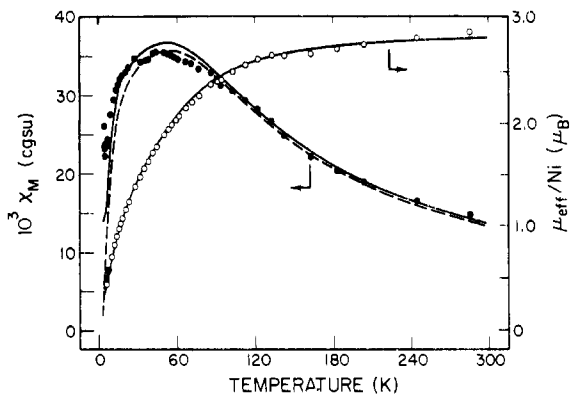

Figure 7. Plots of molar paramagnetic susceptibility per tetramer and effective magnetic moment per nickel(II) ion vs. temperature for $[Ni_4(OCH_3)_4(TMB)_4(OAc)_2](BPh_4)_2$. The dashed line results from a least-squares fit to eq 5 (cubane cluster with unequal exchange parameters) to give $J_1 = -9.1$, $J_2 = 17.7$, and $J_3 = 17.2$ cm^{-1} and $g = 2.00$. The solid line results from correcting for a small amount of a paramagnetic impurity.

1 min under high vacuum the mass spectrum showed the presence almost exclusively of CH_2Cl_2. The modeling of the solvent areas with CH_2Cl_2 initially used 1.77 Å for the C–Cl bond length and 122° for the Cl–C–Cl angle. In the end these constraints were slightly relaxed in order to improve the fit to the data. The final C–Cl bond lengths varied from 1.30 to 1.92 Å, and the bond angles varied from 95 to 124°. The average C–Cl distance was 1.69 Å, and the average Cl–C–Cl angle was 111°.

Spectroscopic Properties. The compound $[Ni_4(OCH_3)_4(TMB)_4(OAc)_2](BPh_4)_2$ shows characteristic infrared bands at 2192 cm^{-1} due to C≡N and at 1567 and 1416 cm^{-1} due to acetate. The electronic absorption spectrum is that of a $^3A_2$ octahedral Ni(II) complex. The maxima and molar absorptivities (ϵ/Ni$_4$) of the three d–d bands ($^3A_2$ to $^3T_2$, $^3T_1$(F), and $^3T_1$(P)) are 850 (85), 580 (45), and ~360 nm (110 M^{-1} cm^{-1}; CH_2Cl_2 solution).

Magnetic Susceptibility. Data taken on a sample of $[Ni_4(OCH_3)_4(TMB)_4(OAc)_2](BPh_4)_2$ are given in the supplementary material, together with susceptibilities calculated with the different theoretical equations. The variation with temperature of χ_M for the cubane cluster is illustrated in Figure 6. The effective magnetic moment per nickel ion, μ_{eff}/Ni, varies gradually from 2.88 μ_B at 286 K to 0.47 μ_B at 4.2 K. All of the $Ni_4(OCH_3)_4^{4+}$ cubane clusters examined previously show an increase in μ_{eff}/Ni as the sample temperature is decreased. It is clear that, in contrast to all other nickel tetramers, the magnetic properties of $[Ni_4(OCH_3)_4(TMB)_4(OAc)_2](BPh_4)_2$ are dominated by an antiferromagnetic exchange interaction. The interaction is most likely *intra*molecular, because the BPh_4^- counterions should afford good *inter*molecular magnetic shielding.

The magnetic susceptibility data for $[Ni_4(OCH_3)_4(TMB)_4(OAc)_2](BPh_4)_2$ were least-squares fit to the three theoretical models discussed above. It can be seen in Figure 6 that neither the cubane model with one exchange parameter, eq 2, nor the noninteracting dimer model, eq 6, adequately reproduces the shape of the experimental curve. Fitting to eq 2 gave $J = -18$ cm^{-1} and $g = 2.16$. As illustrated by the solid line in Figure 6, the cubane model with a single J value does not give a maximum in the χ_M vs. temperature curve as broad as found experimentally. The fit to the noninteracting dimer model is illustrated by the dashed line and gives $J = -10$ cm^{-1} and $g = 2.20$.

The least-squares fit to eq 5 for the cubane model with three different exchange parameters is illustrated in Figure 7. The dashed line results from fitting the susceptibility data to eq

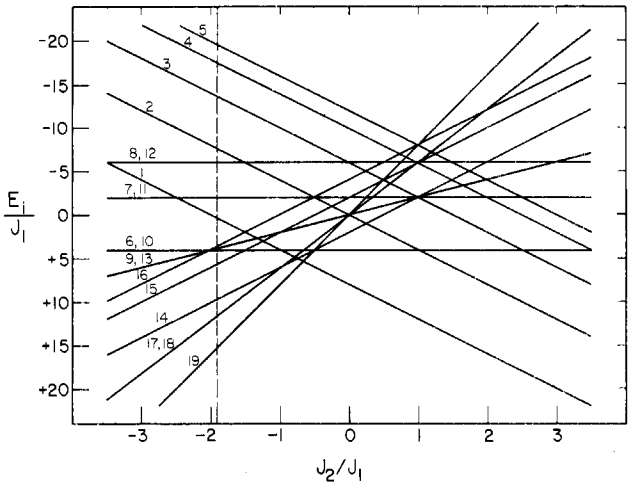

Figure 8. Plot of the energies (divided by J_1) of the 19 electronic states of $[Ni_4(OCH_3)_4(TMB)_4(OAc)_2](BPh_4)_2$ as a function of J_2/J_1 for the cubane theoretical model with unequal exchange parameters. Table II should be consulted to identify the 19 states. The vertical dashed line corresponds to the least-squares fit of the data for the present complex.

5 to give $J_1 = 9.1$, $J_2 = 17.7$, and $J_3 = 17.2$ cm^{-1} and $g = 2.00$. This fit is reasonable despite the fact that there is some deviation at temperatures less than ca. 30 K. The parameters J_2 and J_3 were found not to differ significantly. The fit to the model utilizing three exchange parameters is very sensitive to the magnitude of the antiferromagnetic interaction J_1; however, it is less sensitive to J_2 and J_3 values that characterize the ferromagnetic interaction. The fit to eq 5 can be readily improved by assuming that the sample contains some small amount of paramagnetic impurity. If the magnetic susceptibility of the paramagnetic impurity at 4.2 K is identified as χ_{para}, the magnetic susceptibility of the impurity at any temperature is $4.2\chi_{para}/T$. The solid lines in Figure 7 show how the fit can be improved at low temperatures by taking $\chi_{para} = 0.012$ cgsu together with $J_1 = -9.1$, $J_2 = 17.7$, and $J_3 = 17.2$ cm^{-1} and $g = 2.00$. If the paramagnetic impurity is assumed to have a molecular weight equal to one-fourth that of the TMB cubane complex, this value of χ_{para} corresponds to 4.9% by weight of an impurity.

The unusual magnetic behavior of $[Ni_4(OCH_3)_4(TMB)_4(OAc)_2](BPh_4)_2$ is attributed to the presence of the bridging acetates, which lead to a distortion of the $Ni_4(OCH_3)_4^{4+}$ core that produces two types of Ni–O–Ni angles, those that are ca.

93° and those that are ca. 101°. It is reasonable to suggest that the ~101° Ni–O–Ni angles lead to the antiferromagnetic interaction ($J_1 = -9.1$ cm^{-1}), whereas the ferromagnetic interaction is associated with the ~93° Ni–O–Ni angles (J_2 ($\approx J_3$) of ca. 18 cm^{-1}).

The use of a Weiss constant (Θ) is not apppropriate for fitting the data for $[Ni_4(OCH_3)_4(TMB)_4(OAc)_2](BPh_4)_2$, because the ground state of this complex has $S = 0$. This can be seen from a diagram in which the energies (divided by J_1) of the 19 states of this complex are plotted as a function of J_2/J_1 (Figure 8). In the present complex $J_2/J_1 = -1.92$, which is represented by the vertical dashed line. Level 19 is the ground state; examination of Table III shows that this is the state where all of the electrons are paired.

Acknowledgment. Research at Caltech was supported by National Science Foundation Grant CHE-78-10530. W.L.G. acknowledges a National Science Foundation Postdoctoral Fellowship (1978–1979).

Registry No. $[Ni_4(OCH_3)_4(TMB)_4(OAc)_2](BPh_4)_2 \cdot 4CH_2Cl_2$, 77241-80-6; $[Ni_4(OCH_3)_4(DMB)_4(OAc)_2](BPh_4)_2$, 77241-82-8.

Supplementary Material Available: Tables of solvent parameters and hydrogen parameters from the structure determination, structure factors, and experimental and theoretical magnetic susceptibility data (42 pages). Ordering information is given on any current masthead page.

Contribution from the Michael Faraday Laboratories, Department of Chemistry, Northern Illinois University, DeKalb, Illinois 60115

Fluoro-Containing Complexes of Chromium(III). 10. Preparation, Crystal Structure, and Some Reactions of the *trans*-Fluoroamminebis(1,3-propanediamine)chromium(III) Cation[1]

JOE W. VAUGHN

Received October 22, 1980

The reaction of *trans*-$[Cr(1,3\text{-pn})_2FBr]ClO_4$ (1,3-pn = 1,3-propanediamine) with liquid ammonia at room temperature was used to prepare the *trans*-$[Cr(1,3\text{-pn})_2FNH_3]^{2+}$ cation. The ammination reaction proceeded to yield apparently the trans isomer only. The reaction product with the empirical molecular formula $[Cr(NH_3)F(N_2C_3H_{10})_2](ClO_4)_2$ was subjected to a single-crystal X-ray structural analysis. The complex crystallizes in the monoclinic space group $P2_1/n$ with $a = 10.207$ (4) Å, $b = 9.653$ (4) Å, $c = 17.599$ (5) Å, $\beta = 94.62$ (3)°, $Z = 4$, and $V = 1728$ (1) Å^3. Diffraction data were collected with a computer-controlled four-circle Nicolet autodiffractometer out to a maximum 2θ Mo Kα of 51°. The structure was solved by standard heavy-atom Patterson and Fourier methods and refined by full-matrix least squares. The final discrepancy values based on the 2177 counter data having $I \geq 3\sigma(I)$ were $R_1 = 0.065$ and $R = 0.072$. The final structure revealed that the two chelate rings are nonequivalent in the solid with one of the rings adopting a chair conformation while the other is in a twist conformation. The Cr–F distance is 1.872 (3) Å, and the H_3NCrF angle is 179.0 (2)°. Reaction of the *trans*-FNH_3 complex with more liquid ammonia resulted in little additional ammination, but reaction of the complex with concentrated hydrobromic acid resulted in loss of the fluoro ligand and its replacement by water.

Introduction

In 1975 Wong and Kirk[2] reported the successful preparations of *cis*- and *trans*-$[Cr(en)_2FNH_3]^{2+}$, where en is ethylenediamine, via the reaction of *trans*-$[Cr(en)_2FBr]^+$ with a dilute solution of ammonium perchlorate in dry liquid ammonia at 0 °C. The preparative reaction was accompanied by extensive stereochemical change, and the cis/trans ratio in the crude product was estimated to be 60/40. Previous work in this laboratory[3,4] has indicated that the closely related 1,3-propanediamine complexes are more resistant to stereochemical change than the corresponding ethylenediamine complexes. Hence, the present investigation was undertaken to determine what products would be formed by the reaction of *trans*-$[Cr(1,3\text{-pn})_2FBr]^+$ with liquid ammonia and to characterize these products.

Experimental Section

Caution! Perchlorate salts of metal complexes with reducing ligands such as amines are potentially explosive, and care should be exercised when handling these materials.

Preparation of Starting Material. *trans*-Bromofluorobis(1,3-propanediamine)chromium(III) perchlorate–0.5-water was prepared as described in the literature.[3] A solution of 1.17 g (2.9 mmol) of the crude product in 11 mL of water at 10 °C was prepared and filtered to remove a small amount of undissolved material. Solid sodium perchlorate was added to the stirred filtrate, and the precipitated product was collected, washed with acetone, and air-dried; yield 0.52 g (44%). Anal. Calcd for *trans*-$[Cr(1,3\text{-pn})_2FBr]ClO_4 \cdot 0.5H_2O$: C, 17.7; H, 5.15; N, 13.72. Found: C, 17.79; H, 5.06; N, 13.87.

Preparation of *trans*-Fluoroamminebis(1,3-propanediamine)chromium(III) Bromide Perchlorate. A 3.10-g (7.6-mmol) sample of recrystallized *trans*-$[Cr(1,3\text{-pn})_2FBr](ClO_4) \cdot 0.5H_2O$ was placed in one leg of a modified Y-tube. The tube and its contents were cooled to about −77 °C in a dry ice–2-propanol bath. Gaseous ammonia was added to the cooled reactant until about 25 mL of liquid ammonia had condensed in the tube. The tube was sealed and allowed to stand at room temperature for 2 h. It was necessary to tip the tube several times before the starting material all dissolved in the liquid ammonia. As the starting material dissolved, the solution became deep maroon. After about 1 h at room temperature the solution was deep orange, and red-orange crystals were deposited from the solution. At the end of 2 h the empty leg of the Y-tube was placed in a dry ice–2-propanol bath, and the liquid ammonia was distilled into the cooled leg. The leg containing the liquid ammonia was cut off with a torch and set aside. The leg containing the crude product was opened, attached to a vacuum system, and pumped overnight (0.05 torr, room temperature); yield 3.10 g (98%). The electronic spectrum of the crude material in 0.2 M perchloric acid was characterized by λ_{max} 497 nm (ϵ 46.9 M^{-1} cm^{-1}), λ_{min} 418 (ϵ 13.8), and λ_{max} 366 (ϵ 31.0).

The reaction of *trans*-$[Cr(1,3\text{-pn})_2FBr](ClO_4)$ with liquid ammonia in a sealed tube was repeated as described above except that the temperature of the sealed tube was maintained at 0 °C for the 2-h reaction time. The reaction mixture was worked up as described previously. The electronic spectrum of an aqueous solution of the crude product was characterized by λ_{max} 496 nm (ϵ 47.4), λ_{min} 418 (ϵ 13.6), and λ_{max} 366 (ϵ 30.0). Conversion of the crude product to

(1) Part 9: Vaughn, J. W.; Seiler, G. J. *Inorg. Chem.* **1979**, *18*, 1509.
(2) Wong, C. F. C.; Kirk, A. D. *Can. J. Chem.* **1975**, *53*, 3388.
(3) Vaughn, J. W. *Inorg. Nucl. Chem. Lett.* **1968**, *4*, 183.
(4) DeJovine, J. M.; Mason, W. R.; Vaughn, J. W. *Inorg. Chem.* **1974**, *13*, 66.

0020-1669/81/1320-2397$01.25/0